Vibrations of icosahedron-based networks: Application to amorphous boron

K. Shirai
ISIR, Osaka University 8-1, Mihogaoka, Ibaraki, Osaka 567, Japan

M. F. Thorpe*
Department of Physics and Astronomy, Michigan State University, East Lansing, Michigan 48824
(Received 27 November 1996)

The structure of amorphous boron is believed to be an icosahedron-based random network. The vibrational properties of such a network are studied theoretically using a Bethe lattice of connected icosahedra. The local symmetry of each icosahedron, along with the use of effective fields, greatly reduces the complexity of the problem. We show that many *intra*icosahedral vibrations are not affected by the *inter*icosahedral forces. The peak with the highest frequency, which appears commonly in various spectra of amorphous boron, has been ascribed to the *inter*icosahedral vibrations. It is therefore concluded that the *inter*icosahedral force is stronger than the *intra*icosahedral force. Examination of the density of states at the low-frequency side leads to a relatively large noncentral force for the *inter*icosahedral bond. These conclusions support the view that the *inter*icosahedral bond has a strong covalent character, which is consistent with available experimental data. Raman scattering and infrared absorption are discussed using the shell model and the bond-polarizability model. In these calculations, the spectra are analyzed using the correlations of atomic displacements between different molecular units. [S0163-1829(97)04618-3]

I. INTRODUCTION

Many amorphous semiconductors are characterized by highly oriented covalent bonds. A consequence of this character is that the coordination number of the nearest neighbors is limited to no more than four.[1] Amorphous boron is however an unusual and exceptional case. From optical and electrical properties, amorphous boron can be classified as a semiconductor,[2] due for example to the existence of an optical gap and the temperature dependence of the conductivity.[3–5] In spite of this, structural studies using x-ray and neutron diffraction have shown that the coordination number varies from about five to six.[6] Comparison of such data with a structural model shows that the short-range order of the random network is quite similar to that of an icosahedron.[7] In the case of crystalline boron, the icosahedron is the basic building block of the structure.[8] Hence, we find it useful to model amorphous boron by using a random network composed of icosahedra.

Furthermore, it has become evident that there is a strong correlation in the dihedral angle between adjacent icosahedral units.[9] This is consistent with the existence of a highly oriented bond between adjacent icosahedra. This is quite reasonable, using crystalline boron as a guide, where the semiconducting character arises from the *inter*icosahedral bonds.[8,10] In this way, it is thought that strong *inter*icosahedral bonds form covalent bonds for the amorphous state too, which give rise to the semiconducting character. This differentiates amorphous boron from quasicrystals possessing icosahedral structures, where the interactions between the icosahedral units are much weaker.

In addition to structural studies, recently vibrational spectra have been examined for amorphous boron, using infrared and Raman spectroscopy,[11–13] and inelastic neutron scattering.[14] Accordingly, we are now in position to be able to begin to discuss quantitatively the nature of vibrations in icosahedron-based networks.

It would not be easy to construct a model in which all space is completely filled with a random network of interconnected icosahedra. Therefore, as a first study, we have adapted the Bethe lattice model.[15] Such a model has been used in amorphous silicon,[16] vitreous quartz, and other amorphous solids.[17,18] The usual Bethe lattice is an infinite treelike sequence of branches and nodes. The node is regarded as a simple point, but for the present problem we introduce the molecularlike internal structure of the icosahedron at each node. This structure may be thought of as a Bethe lattice with a basis in analogy with crystal structures. In the present problem the basis is the icosahedron. This Bethe lattice model emphasizes the short-range order of the molecular unit, but is still fully connected. The present network is more akin to the Husimi cactus used for studies of magnetism.[19]

From a theoretical standpoint, this Bethe lattice model has some advantages. One is the use of the local icosahedral symmetry of the molecular unit, which considerably simplifies the dynamical problem. This technique has been partly developed in a previous paper for obtaining the vibrational density of states (DOS).[20] In this current paper, we have fully developed the symmetry technique in order to extend the formulas to optical properties. In calculating optical spectra, long-range correlation must be taken into account in some way. In treating long-range correlations via the Bethe lattice model, it is noted that there is an intrinsic problem with the model, i.e., the divergence of the sums involving long-range correlation.[21,22] We do not intend to reexamine this problem here, but will truncate the summation as was done previously.[21,22] These theoretical aspects of the model are discussed in the next section. The application to the icosahedral Bethe lattice is then discussed in Sec. III. Comparisons

 © 1997 The American Physical Society

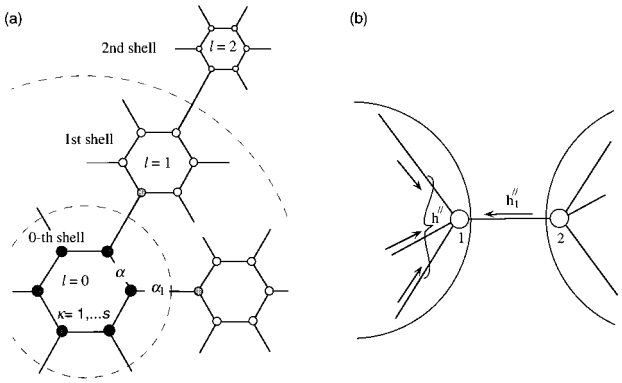

FIG. 1. A model of the Bethe lattice possessing a molecular unit. The lattice site l is classified by the shell. In discussing optical properties, black atoms of the zeroth shell have the dominant contribution, and the contribution of the gray atoms in the first shell is the leading correction. (b) The effective fields and the interaction between the nearest-neighbor atoms in the adjacent molecular units.

of our results with the experimentally measured DOS, infrared spectra, and Raman spectra are made throughout the paper.

II. THEORY OF THE BETHE LATTICE WITH A BASIS

Let us first consider a general model of the Bethe lattice which has a molecular unit composed of s atoms of the same chemical element as the basis. Each molecular unit has z nearest neighbors. Here, we consider the simplest case $z=s$. Let m be the mass of the atom. Similar to the crystalline case, we can label all the atoms by a lattice site l and by an atom site κ from the basis, $\kappa=1,\ldots,s$ (see Fig. 1). The number of the lattice sites N is, of course, fairly large. The Green's function $\mathcal{G}(\kappa\kappa)=\mathcal{G}(l\kappa;l\kappa)$ for this problem can be written

$$\mathcal{G}_{\mu\mu}(\kappa\kappa)=\sum_{q}^{3Ns}\frac{|\langle l\kappa\mu|q\rangle|^2}{m(\omega^2-\omega_q^2)}, \tag{2.1}$$

with use of all the eigenfrequencies ω_q. Note that q labels the eigenstates and is *not* a momentum tag, as the system has no crystalline periodicity. To obtain all the eigenfrequencies is difficult, however with the help of an effective field, the exact solution of this problem can be found.[15]

We introduce the *intra*molecular and *inter*molecular central forces, α and α_1, respectively. For noncentral forces, there are several choices, such as the valence force model, Keating model,[23] etc. For the *intra*molecular-angle force β, we can manage any model, no matter how complex. However, for the *inter*molecular–angular force constant β_1, the Born form is the only model which is practically and analytically manageable in the Bethe lattice problem.

Let us suppose that atom 1 at the left-hand lattice site is connected to atom 2 at the right-hand lattice site [Fig. 1(b)]. All the influence from the left-hand side to atom 1 can be expressed by the effective field $h^{\parallel}$, which acts parallel to the bond 1-2. On the other hand, atom 1 is also subjected to the influence of atom 2, which has the same effective field $h^{\parallel}$. The influence on atom 1 from the right-hand side through the parallel direction, $h_1^{\parallel}$, is then given by

$$h_1^{\parallel}=\alpha_1+\frac{{\alpha_1}^2}{m\omega^2-\alpha_1-h^{\parallel}}. \tag{2.2}$$

By using these two fields, the total field $h_t^{\parallel}$ acting on atom 1 from both sides becomes $h_t^{\parallel}=h^{\parallel}+h_1^{\parallel}$. The parallel component of the Green's function $\mathcal{G}^{\parallel}=\mathcal{G}_{zz}(11)$ is immediately diagonalized to give

$$\mathcal{G}^{\parallel}=\frac{1}{m\omega^2-h_t^{\parallel}}. \tag{2.3}$$

Similar equations hold for the perpendicular components $\mathcal{G}^{\perp}$ and $h_t^{\perp}$.

Among these effective fields, only two are independent; say, $h_1^{\parallel}$ and $h_1^{\perp}$. Now, the problem is how to determine these fields. Let us consider a molecular unit in the Bethe lattice. We disconnect the unit under question from all the other units, and replace the *inter*molecular bonds with dangling bonds which have associated fields $h_1^{\parallel}$ and $h_1^{\perp}$. The dynamical problem is then reduced to $3s\times 3s$ dimensions, but note that the dynamical matrix is a function of complex fields. The formal $3s$ solutions $\omega_r(h)$ give a complete spectrum of the eigenfrequencies through the Green's function, which is given by

$$\mathcal{G}_{\mu\mu}(\kappa\kappa)=\frac{1}{m}\sum_{r}^{3s}\frac{|\langle\kappa\mu|r\rangle|^2}{\omega^2-\omega_r(h)^2}, \tag{2.4}$$

where $|r\rangle$ is the eigenvector of the dynamical matrix of $3s\times 3s$ dimensions. Here, $\omega_r(h)$ represents that ω_r is a function of both $h_1^{\parallel}$ and $h_1^{\perp}$. By equating Eqs. (2.3) and (2.4), we can determine the effective field $h_1^{\parallel}$. This is a self-consistent equation.[15] There are two such self-consistent equations for the parallel and perpendicular components. In general, $h_1^{\parallel}$ and $h_1^{\perp}$ enter in both equations which are coupled via $\omega_r(h)$. When either α_1 or β_1 is ignored, the parallel and perpendicular components become decoupled. We may regard r as the label of the irreducible representations, when the dynamical matrix is block diagonalized by symmetry.

Optical properties. Optical properties are related to the long-range correlation of atomic displacements, because of the long-wavelength nature of light (when compared to interatomic distances). In terms of Green's functions, optical properties are evaluated by a summation of the type $\Sigma_{\kappa\mu}\Sigma_{l'\kappa'\nu}\mathcal{G}_{\mu\nu}(0\kappa;l'\kappa')$ with appropriate matrix elements. This can be handled in a straightforward manner in crystals, leading to the usual $k=0$ momentum selection rules. It causes considerable difficulty in Bethe lattice type calculations.[21,22] These difficulties have not been fully resolved at the present time, but are not the topic of this paper. We follow the spirit of previous work which has been quite successful in simpler structures.[22] We divide the summation into pieces over shells, depending on the distance of the lattice site l' from the origin; the zeroth shell refers merely to the lattice site of the origin, the first shell is composed of z nearest-neighboring (icosahedral) units, etc. [see Fig. 1(a)]. For the zeroth shell, the summation is rewritten as

$$\sum_{\kappa\mu}\sum_{\kappa'\nu}\mathcal{G}_{\mu\nu}(0\kappa;0\kappa')=\frac{1}{m}\sum_{r}^{3s}\frac{1}{\omega^2-\omega_r(h)^2}, \quad (2.5)$$

from a relationship between Eqs. (2.1) and (2.4) and the orthogonality of the eigenvector $|0\kappa\mu\rangle$. For more distant shells, we can reduce the formula to a tractable form by using a transfer matrix relating the displacement $|l\kappa\mu\rangle$ to that of the adjacent lattice site $|l'\kappa'\nu\rangle$. The transfer matrix $\mathbf{T}$, which is a function of the fields, has a dimension $3s$. Finally, the summation is given by

$$\sum_{\kappa\mu}\sum_{l'\kappa'\nu}\mathcal{G}_{\mu\nu}(0\kappa;l'\kappa')=\frac{1}{m}\sum_{r}^{3s}\frac{1}{\omega^2-\omega_r(h)^2}\sum_{\kappa\mu}\sum_{\kappa'\nu}\sum_{\kappa''\lambda}\langle 0\kappa\mu|r\rangle\{\mathbf{1}+z\mathbf{T}+(z\mathbf{T})^2+\cdots\}_{\kappa'\nu,\kappa''\lambda}\langle r|0\kappa''\lambda\rangle. \quad (2.6)$$

This sum does not converge for $z>2$, because of the unphysical (large) surface of the Bethe lattice.[15,21] Therefore to truncate *or* to introduce a weighting factor such as an exponential decay is necessary. Such an artifact is reasonable for amorphous materials because of the lack of long-range order. Hence, we adopt such an approach here, and in the following calculations, we will terminate the summation after two terms:

$$\frac{1}{m}\sum_{r}^{3s}\frac{1}{\omega^2-\omega_r(h)^2}+\sum_{\kappa\mu}\sum_{\kappa'\nu}\mathcal{G}_{\mu\nu}(0\kappa;1\kappa'). \quad (2.7)$$

The summation in the last term is understood to involve only those atoms in the first shell which are directly joined to the zeroth shell [gray atoms in Fig. 1(a)].

The infrared absorption is described by the dielectric susceptibility $\chi_{\mu\nu}(\omega)$, which is given by

$$\chi_{\mu\nu}(\omega)=-\sum_{l\kappa\mu'}\sum_{l'\kappa'\nu'}e_{\mu\mu'}(\kappa)e_{\nu\nu'}(\kappa')\mathcal{G}_{\mu'\nu'}(l\kappa;l'\kappa'), \quad (2.8)$$

where $e_{\mu\nu}(\kappa)$ is the effective charge tensor of the κth atom [see Ref. 24, Eq. (1.15)]. The absorption coefficient K is obtained by $K=4\pi\omega$ Im $\chi/(\eta c)$, where η is the refractive index of the sample and c is the speed of light. In a similar way, this summation (2.8) is approximated by two terms:

$$\chi_{\mu\nu}(\omega)=\sum_{r}^{\mathrm{IR}}\sum_{i}^{n_r}\frac{Q_i(r)^2}{\omega_{ri}(h)^2-\omega^2}-\sum_{\kappa\mu'}\sum_{\kappa'\nu'}e_{\mu\mu'}(\kappa)e_{\nu\nu'}(\kappa')\mathcal{G}_{\mu'\nu'}(0\kappa;1\kappa'), \quad (2.9)$$

where the summation of the first term is taken only for the infrared active modes with rth symmetry, which comprises a set of n_r normal modes within the molecular (icosahedral) unit. Here, $Q_i(r)$ is the effective charge for the ith mode of the rth symmetry. In obtaining Eq. (2.9), use is made of the orthogonality property of the effective charges.[25]

For Raman scattering, the scattering efficiency is expressed as a fourth-rank tensor $I_{\alpha\gamma,\beta\lambda}(\omega)$, which is given by

$$I_{\alpha\gamma,\beta\lambda}(\omega)=\sum_{\kappa\mu}\sum_{l'\kappa'\nu}P_{\alpha\gamma,\nu}(l'\kappa')P_{\beta\lambda,\mu}(0\kappa)\mathrm{Im}\mathcal{G}_{\mu\nu}(0\kappa;l'\kappa'), \quad (2.10)$$

where the $P_{\alpha\beta,\mu}(l\kappa)$ are the derivatives of the polarizability with respect to the displacements $|l\kappa\mu\rangle$ [see Ref. 24, Eq. (4.12)]. The Bose factor is omitted here for convenience. To the same order of approximation as Eq. (2.7), the sum (2.10) becomes

$$I_{\alpha\gamma,\beta\lambda}(\omega)=\mathrm{Im}\sum_{r}^{\mathrm{Raman}}\sum_{i}^{n_r}\frac{R^r_{\alpha\beta}R^r_{\gamma\lambda}}{\omega^2-\omega_{ri}(h)^2}+\sum_{\kappa\mu}\sum_{\kappa'\nu}P_{\alpha\gamma,\nu}(l'\kappa')P_{\beta\lambda,\mu}(l\kappa)\mathrm{Im}\,\mathcal{G}_{\mu\nu}(0\kappa;1\kappa'), \quad (2.11)$$

where the $R^r_{\alpha\beta}=\Sigma_{\kappa\mu}P_{\alpha\beta,\mu}\langle l\kappa\mu|r\rangle$ are usual the second-rank Raman tensors. The summation in the first term is taken over all the Raman-active modes.

III. APPLICATION TO AN ICOSAHEDRAL BETHE LATTICE

Now, let us look at the detailed problem of the icosahedron-based network, and apply the theory given in the previous section to the icosahedral Bethe lattice. In a previous paper,[20] we sought the solution under the very restricted condition of central forces α and α_1 only. Here, we have sought the solution under more general and hopefully realistic conditions, i.e., noncentral forces of the *intra*icosahedral β and the *inter*icosahedral β_1 are included. For boron solids, however, there is a reason that the *intra*icosahedral force β can be ignored. It becomes clear, from the study of lattice vibrations of various crystalline borons, that the angle-bending force of the *intra*icosahedral bond is very small[25,26] or (surprisingly) even negative.[10] This is partly because of the electron-deficient property of boron, and partly because of the intrinsic instability of polyhedral molecules in a similar way to the Jahn-Teller instability. Hence, we ignore β in the present problem. On the other hand, the *inter*icosahedral

bonds of boron crystals are covalent, and so it is reasonable to assume a relatively large angle-bending force β_1.[10] For the Bethe lattice, only the Born model is usable in the present mathematical manipulation. However it is known that Born forces mimic the more realistic Keating or valence forces quite closely.

Accordingly, we use three parameters, α, α_1, and β_1. Throughout this paper, we use set $\alpha=1$ for convenience. For the boron case, the frequency 1 in this unit corresponds to 395 cm^{-1} in reality, so this sets the scale factor. According to the procedure described in Sec. II, the dynamical matrix is reduced to 36×36, and is further reduced by the icosahedral symmetry to block diagonal form as $A_g+T_{1g}+2T_{1u}+T_{2u}+U_g+U_u+2V_g+V_u$. Out of these, T_{1u} is infrared active, whereas A_g and V_g are Raman active. By taking the coordinates in a way that the fivefold axis around atom 1 is taken as the z axis (a convention that is used throughout this paper) many symmetry vectors have value zero for the $|1z\rangle$ component, and thereby many terms in the summation (2.4) can be dropped.

We are now left to solve the self-consistent equations, which are two simultaneous equations with two unknowns, say, $h_1^{\parallel}$ and $h_1^{\perp}$. In terms of real variables, we have to solve four simultaneous equations of polynomials with four unknowns, the degree of polynomials being more than 16. Such problems can be numerically solved by an iterative method.

Although the final spectra are always obtained by using all the force constants in the model, frequently use is made of the simpler limiting case of the two-force constant model (α and α_1 only). When the two-force constant model is used, the self-consistent equations are reduced to a single equation with respect to the parallel components. In this case, to solve the equation and to determine the physical solution is a simple task.

A. Density of states

As usual, the DOS $\rho(\omega)$ is given by

$$\rho(\omega)=-\frac{2\omega}{m\pi}\,\mathrm{Im}\left\{\sum_r^{3s}\frac{1}{\omega^2-\omega_r(h)^2}\right\}. \tag{3.1}$$

Let us first consider the simplest case of central forces only, and examine the development of the DOS when the *inter*icosahedral force α_1 is varied from the case of an isolated molecule to that of a continuous network. In Fig. 2, the evolution of the DOS as a function of α_1 is shown. Since the parallel component of the self-consistent equation has two singlets A_g and T_{1u} and two doublets T_{2u} and V_g only, all the remaining modes are δ functions. We broaden these δ function modes by introducing an imaginary part in the frequency, i.e., $\varepsilon=0.02$. The limiting case of an isolated icosahedral molecule, $\alpha_1=0$, is shown at the bottom portion by a line spectrum. At the top of the figure, we show the final result obtained by using the full parameters, which is compared with the experimental spectrum of the inelastic neutron scattering for amorphous boron.[14] In order to fit to experiment, $\alpha=1.2$ (mdyn/Å) is used, and the real value of the frequency is shown in the top panel.

It is interesting to see in the figure that most of the eigenfrequencies do *not* change significantly with α_1, except the highest and lowest frequency bands. This is true not only in the molecular crystal limit ($\alpha_1\ll\alpha$), but also for the opposite extreme ($\alpha_1\gg\alpha$). Because the central force α_1 acts on the icosahedron effectively only parallel to the *inter*icosahedral bond, *intra*icosahedral vibrations which have no component in this direction are not affected by α_1. These *intra*icosahedral modes coalesce into a broad band ranging from $\omega=0.7$ to 1.85, when disorder is introduced. Thus, we may regard a broad band from 400 cm^{-1} up to 1000 cm^{-1} in the experiment as originating from the *intra*icosahedral vibrations.

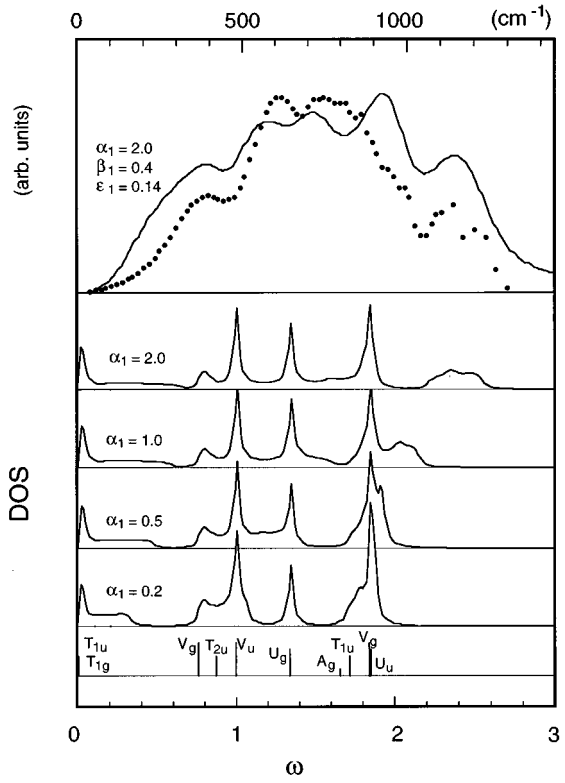

FIG. 2. Showing the evolution of the DOS. Except for the top panel, the intericosahedral force α_1 increases upward from the bottom, with $\varepsilon=0.02$ and $\beta_1=0$. The top panel shows the final calculation using the full parameters: $\alpha_1=2.0$, $\beta_1=0.4$, $\varepsilon=0.14$, relative to α. The spectrum is compared with a neutron scattering experiment (Ref. 14) indicated by dots. For comparison with experiment, the value, $\alpha=1.2$ (mdyn/Å) is used.

On the other hand, higher frequency bands, which arise from A_g, T_{1u}, and V_g in the isolated icosahedron, move to higher frequencies as α_1 is increased, and are singled out from the continuous band for $\alpha_1>1$. This may correspond to the secondary feature appearing around 1100 cm^{-1} in the experiment. The result that the *inter*icosahedral force is twice the *intra*icosahedral force is quite reasonable, considering the crystal case.[26] Also in the amorphous state, the *inter*icosahedral bond has covalent character, as mentioned in Sec. I, and hence it is reasonable to use a strong force for this bond.

Agreement between the calculation and the experiment is quite satisfactory overall, as shown in the top of Fig. 2. In a previous paper,[20] we used only central forces. In that case, a peak remains at low frequencies, $\omega<100$ cm^{-1} (see Fig. 3 of Ref. 20), where there is no such peak in the experiment. This

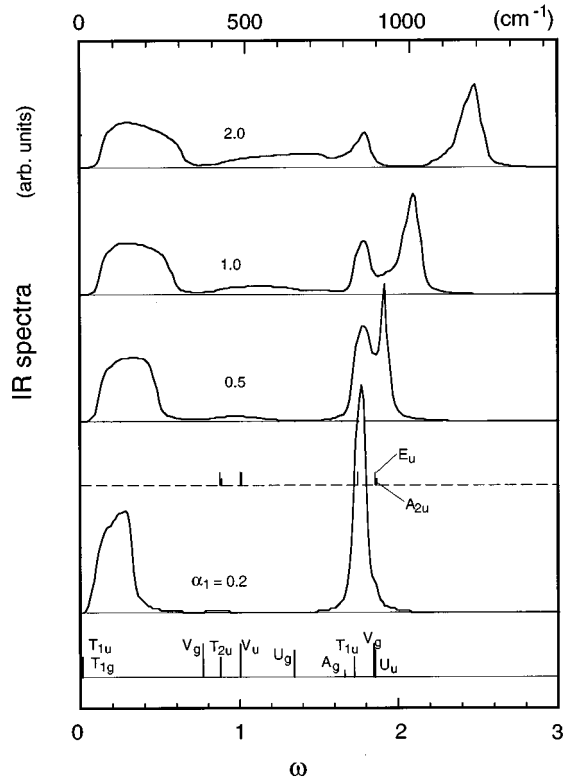

FIG. 3. Evolution of the infrared activity using the two-force-constant model, with a broadening parameter $\varepsilon = 0.02$. The zone-center modes of crystalline boron are shown by the line spectra for comparison. The infrared active modes of the crystal are essentially independent of α_1. The value 1.2 (mdyn/Å) is used for α.

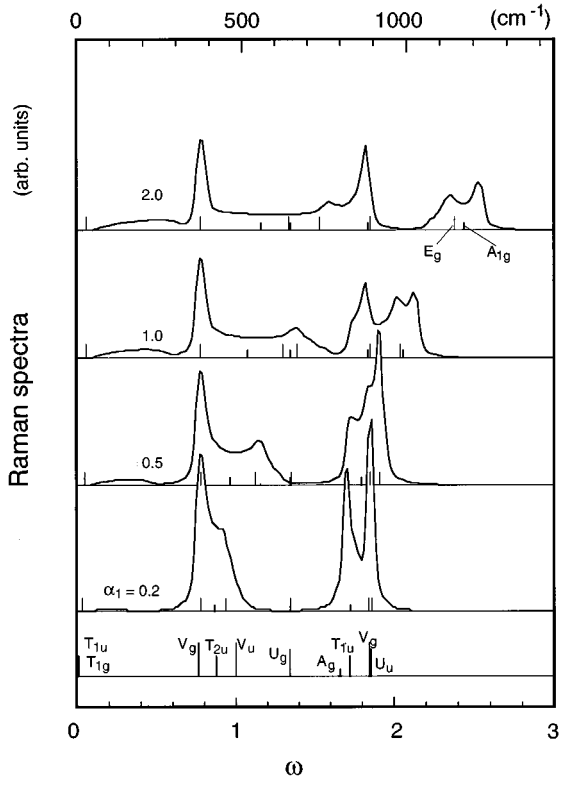

FIG. 4. Evolution of the Raman activity using the two-force-constant model. The zone-center modes of the crystal boron are shown by the line spectra for comparison. The parameters are the same as in Fig. 3.

peak arises from the acoustic T_{1u} and the rotational T_{1g} modes of the icosahedral molecule. The librational mode T_{1g} has a zero frequency (floppy mode) when β_1 is neglected. When β_1 is introduced, the librational modes have a finite frequency, and the acoustic modes have a dispersion, which eliminates the unrealistic peak. Therefore, a gradual increase in the DOS with ω at the low-frequency side can be regarded as evidence of a relatively large noncentral force for the *inter*icosahedral bonds.

B. Optical spectra

As described in Sec. II, the first terms in Eqs. (2.9) and (2.11) give a usable approximation for the optical properties. Let us first evaluate the infrared and Raman spectra using this approximation, and simply ignoring the matrix elements. For the infrared spectra, the summation is a single term of T_{1u}. For the Raman spectra, the summation consists of a singlet A_g and a doublet V_g possessing fivefold degeneracy. The correction due to the first shell will be investigated latter. To see how the spectra develop from the isolated molecule, we initially used the two-force constant model. The results are shown in Fig. 3 for the infrared spectra and in Fig. 4 for the Raman spectra. For the infrared spectra, a prefactor ω is included in order to compare with the absorption coefficient. Comparison is made with the lattice vibrations of the crystal boron (α boron). The symmetry of the crystal has been lowered to D_{3d}. Topologically, the structure of crystalline α boron is similar to our model of the icosahedron-based network. But, in the crystal case, only half of the atoms out of the 12 icosahedral atoms have the nearest-neighbor icosahedron; i.e., $z = 6$ while $s = 12$. The zone-center vibrations of the crystal are shown by line spectra in Figs. 3 and 4. Detailed analyses of the crystal spectra are described in Refs. 25 and 26.

Because $z < s$ for the crystal, the frequencies are, on average, smaller than those of the icosahedral Bethe lattice, as shown in Figs. 3 and 4. However, it is interesting to note that both the highest infrared and the Raman bands in the Bethe lattice increase in frequency with increasing α_1, although in the crystal case the infrared active modes are essentially independent of α_1. The difference can be explained by considering the contribution of the *inter*icosahedral bonds.

In the crystal case, the center of the icosahedron is also a center of inversion. For infrared active modes, the pair of atoms whose locations are interchanged by inversion, vibrate antisymmetrically. The nearest-neighbor atom in the adjacent unit, accordingly, vibrates antisymmetrically for the zone-center modes (see the left-hand side of Fig. 5). Of course, those zone-center modes are the only modes which are observed in the spectra. There is no contribution to the frequency from the force constant α_1. For Raman-active modes, on the contrary, the opposite-site atoms with respect to the inversion center, vibrate symmetrically, and also for a pair of atoms of an intericosahedral bond. The effect of α_1 is maximized in this configuration. This is why the top Raman band is appreciably higher than the top infrared band in the crystal boron.

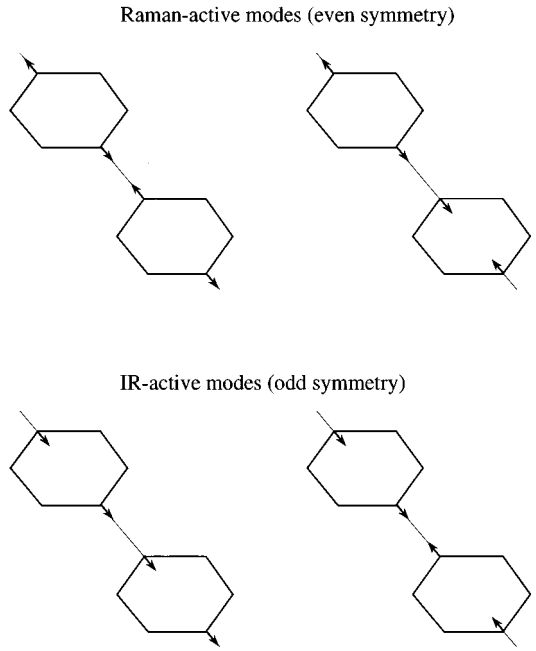

FIG. 5. The highest infrared and Raman-active modes of crystalline boron. The zone-center modes (the left-hand side) are compared to those of the zone boundary (the right-hand side).

Going towards the zone boundary, those symmetrical and antisymmetrical vibrations of the *inter*icosahedral bond are interchanged (the right-hand side of Fig. 5). The frequency of the Raman branch is decreased, while that of the infrared branch is increased. As a consequence, these two frequencies averaged over all the zone become almost the same. Actually, the experimental infrared and Raman spectra of amorphous boron have a secondary feature around 1100 cm^{-1}, which will be seen later.

For comparing with experimental spectra, it is necessary to consider the matrix elements and to correct the spectra by taking the influence of further-distant shells into account. The following subsections are addressed to these issues.

1. Infrared spectrum

Even for those solids which are composed of the same chemical elements, infrared active modes can occur. The dynamic and distortion effect of the charge distribution is the cause of the infrared activity.[27] To describe this situation, a tensor expression for the effective charge is used. Such tensors are subjected to the strict requirement of the local symmetry. The form of the tensor for the icosahedral molecule is given in Ref. 25, and is used in this study. Another form of this tensor which is frequently used for amorphous solids is the Alben model.[28] In that model, the symmetry restrictions are relaxed; only general requirements, such as the rotational invariance, are assumed. Comparison between these two forms are discussed elsewhere.[29]

For an icosahedral molecule, there is only one infrared active mode, T_{1u}, and accordingly the effective charge tensors have only one independent parameter. In terms of the shell model,[25] the effective charge of this mode Q^* is given by $-\sqrt{12}a_{12}Z$, where Z is the shell charge and a_{12} is an appropriate coupling constant between the core and shell

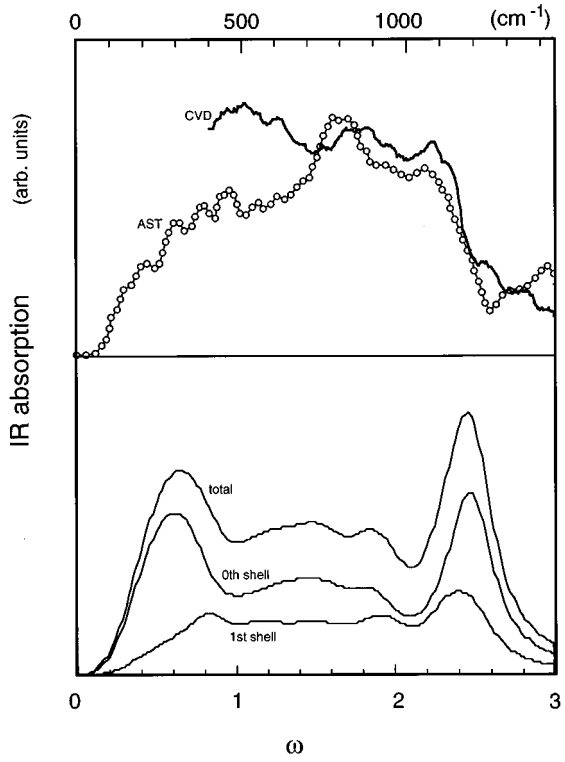

FIG. 6. The final calculation of the infrared absorption spectrum, compared with experiments. Each contribution from the zeroth and first shells, the total absorption, are separately plotted. The parameters are $\alpha_1=2.0$, $\beta_1=0.4$, $\varepsilon=0.14$, relative to α. For real values, $\alpha=1.2$ (mdyn/Å) is used. Two experimental spectra are quoted in different forms of samples: a film (CVD) (Ref. 13) and a powder sample (AST) (Ref. 12).

motions. On converting the normal coordinates to the Cartesian coordinates, the longitudinal component $e_\parallel$ of the effective charge of atom 1 is given by $\sqrt{2}a_{12}Z$. The transverse component $e_\perp$ is equal to $-e_\parallel/2$. The contribution from a pair of atoms in an *inter*icosahedral bond, $\Sigma_{\mu'\nu'}e_{\mu\mu'}(1)e_{\nu\nu'}(2)\mathcal{G}_{\mu'\nu'}(01;12)$, is then diagonalized along the z direction, whose parallel component is given by $(e_\parallel)^2\mathcal{G}'_\parallel$ and the perpendicular component is given by $(e_\perp)^2\mathcal{G}'_\perp$. Here, we use a shorthand, $\mathcal{G}'_\parallel=\mathcal{G}^\parallel(21)$ and $\mathcal{G}'_\perp=\mathcal{G}^\perp(21)$. The other contributions are readily obtained by symmetry. The contribution from the whole of the first shell, as well as that from the zeroth shell, becomes isotropic, as expected. The final form of the dielectric susceptibility is given by

$$\chi(\omega)=4(a_{12}Z)^2\left\{\frac{1}{M}\frac{3}{\omega_{T_{1u}}(h)^2-\omega^2}-(\mathcal{G}'_\perp+2\mathcal{G}'_\parallel)\right\}. \quad (3.2)$$

The first and second terms in parentheses correspond to the contributions from the zeroth and first shells, respectively.

In Fig. 6, the absorption coefficient calculated by Eq. (3.2) and the contribution of the zeroth and first shells are indicated. The parameters are the same as those of the top figure of Fig. 2. In Fig. 6 are also shown the spectra of amorphous borons in different forms; a thin film (denoted by CVD) (Ref. 13) and powders (AST).[12] These spectra are basically similar. There is the primary continuous band from

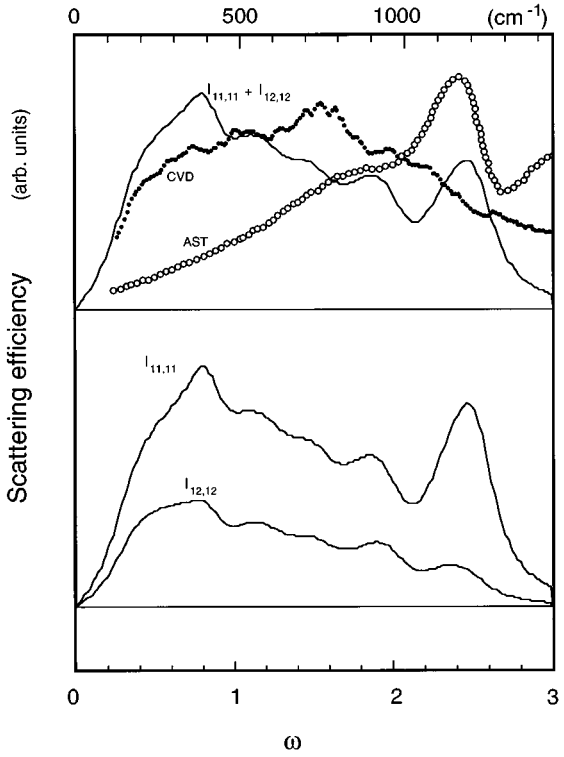

FIG. 7. The calculated polarization characteristics of the Raman scattering. The total scattering efficiency is compared with the experiments of a film (CVD) (Ref. 13) and a powder sample (AST) (Ref. 12). The parameters are the same as those in Fig. 6. The experimental intensity is shown by removing the Bose factor.

400 cm^{-1} up to 1000 cm^{-1}, which has a maximum at around 800 cm^{-1}. As in the inelastic neutron scattering, a secondary band around 1100 cm^{-1} is identified.

These basic features are reproduced in the present calculation. The broad continuous bond has a small peak around 800 cm^{-1}, which originates partly from the infrared active T_{1u} mode of the isolated icosahedral boron molecule. However, the highest band about 1100 cm^{-1} and the lowest band about 300 cm^{-1} are more intense than those of the experiments. These two are ascribed to the highest infrared active T_{1u} mode and to the acoustic branch, respectively, and thereby a large absorption intensity is expected.

As shown in the calculated spectra, the contribution from the zeroth shell is dominant. The influence from the first shell is not very significant. Roughly speaking, the second contribution in Eq. (3.2) reflects the total DOS, while the first term emphasizes the infrared active zone-center modes.

2. Raman spectrum

The transformation property of the fourth-rank tensor $I_{\alpha\gamma,\beta\lambda}$ is the same as that of the elastic constants $c_{\alpha\gamma,\beta\lambda}$. Since the icosahedral symmetry is higher than the cubic symmetry, the symmetry of $I_{\alpha\gamma,\beta\lambda}$ is the same as the isotropic case. Hence, they have only two independent components, that is, $I_{11,11}$ and $I_{12,12}$. These correspond to those experimental situations, which are called the HH and HV configurations. Correspondingly, there are two independent parameters, say a for A_g and b for V_g, in the second-rank Raman tensors for the icosahedral symmetry. The form of the second-rank tensor is determined by symmetry, which is given in Ref. 30. The value of these two parameters can be calculated by the bond-polarizability model, where axial symmetry is assumed for each bond.[31,32] Two bond polarizabilities, $\alpha_{\parallel}(R)$ and $\alpha_{\perp}(R)$, are used and are functions of the bond length R. For an isolated icosahedral molecule, the two parameters are calculated to be,

$$a = -\sqrt{\frac{10(5-\sqrt{5})}{3}}\,\alpha_d(R)',$$

$$b = -\sqrt{\frac{10(5+\sqrt{5})}{10}}\,\alpha_d\left(\ln\frac{\alpha_d}{R^2}\right)', \tag{3.3}$$

where the prime denotes the derivative with respect to R and $\alpha_d(R)=\alpha_{\parallel}(R)-\alpha_{\perp}(R)$.[30]

For the polarizabilities of the *inter*icosahedral bond, different parameters, γ, should be used. In this way, we can obtain the formulas for the scattering efficiency as

$$I_{11,11}(\omega)=\mathrm{Im}\left\{\frac{a^2}{\omega^2-\omega_{A_g}(h)^2}+\frac{4}{3}\sum_i^2\frac{b^2}{\omega^2-\omega_{V_g i}(h)^2}\right\}+\mathrm{Im}\,\frac{4}{5}\left\{(3(\gamma')_{\parallel}^2+4(\gamma')_{\parallel}(\gamma')_{\perp}+8(\gamma')_{\perp}^2)\mathcal{G}_{\parallel}'+8\left\{\frac{\gamma_d}{R}\right\}^2\mathcal{G}_{\perp}'\right\},$$

$$I_{12,12}(\omega)=\mathrm{Im}\left\{\sum_i^2\frac{b^2}{\omega^2-\omega_{V_g i}(h)^2}\right\}+\mathrm{Im}\,\frac{4}{5}\left\{(\gamma_d')^2\mathcal{G}_{\parallel}'+6\left\{\frac{\gamma_d}{R}\right\}^2\mathcal{G}_{\perp}'\right\}. \tag{3.4}$$

The first and second terms on the right-hand side correspond to the contributions from the zeroth and first shells, respectively.

Accordingly, we have five parameters for the bond polarizabilities. Experimentally, there are only two independent polarization characteristics possible. Therefore, we did not try to find all the combinations of the parameters which fit the experiment. What is more disconcerting in the experimental data is that there is a significant discrepancy in the Raman spectra of amorphous boron. This is shown in the top of Fig. 7. Even though these two samples gave similar spectra for the infrared absorption, the Raman spectra are different. The difference may be caused by the laser frequency used for the excitation. For the spectrum of a CVD film, the usual Ar laser (488 nm) was used,[13] while a low frequency laser (1.06 μm) was used for an AST sample.[12] The authors in Ref. 12 recently showed Raman spectra of boron-rich solids different from those obtained by a more traditional

method.[33] This issue is currently unresolved. In spite of this discrepancy, there is a common feature in both spectra in that there is again a secondary peak around 1100 cm^{-1}.

In Fig. 7, an example of the calculated polarization characteristics is shown in the lower panel. The bond polarizabilities used are $\alpha_d(R)'=0.8$, $\alpha_d(R)/R=0.5$, $\gamma_\parallel(R)'=1.6$, $\gamma_\perp(R)'=0$, and $\gamma_d(R)/R=0.8$. The force constants are the same as those in Fig. 2. The sum of these two components is drawn in the top of Fig. 7. The calculated total scattering efficiency is similar to the CVD spectrum in that there is broad continuous band below 1000 cm^{-1}, and is similar to the AST spectrum in that the highest band is clearer.

In obtaining these polarizabilities, we have investigated the following issues. First, large polarizabilities are assumed for the *inter*icosahedral bonds, compared with those of *intra*icosahedral bonds. In general, there is a trend that the scattering efficiency of semiconductors is larger than that of metals. Hence, the above assumption is qualitatively reasonable, considering the covalent character of the *inter*icosahedral bonds. This means that the contribution from the first shell is greater than that of the zeroth shell, compared to situation with the infrared spectra. As a consequence, the Raman spectra more closely reflect the total DOS than the infrared spectra. Second, we assumed that the polarizabilities γ of the *inter*icosahedral bonds are more anisotropic than those of the *intra*icosahedral bonds α. In the second brackets in both $I_{11,11}$ and $I_{12,12}$ in Eq. (3.4), the perpendicular component $\mathcal{G}'_\perp$ gets more weight than $\mathcal{G}'_\parallel$ for the present parameters. Since the perpendicular component $\mathcal{G}'_\perp$ has more low-frequency modes, the contribution from the first shell emphasizes the low-frequency side of the spectrum.

IV. CONCLUSIONS

By using a model of the icosahedral Bethe lattice, we have made a study of the vibrational properties of icosahedron-based random networks. Amorphous boron is the only example of an amorphous semiconductor which is based on such a structure.

Most of the *intra*icosahedral vibrations with intermediate frequencies are not affected by the *inter*icosahedral central force α_1, and form a continuous band in the amorphous state. Only the highest A_g, V_g, and T_{1u} modes are affected by α_1. If $\alpha_1>\alpha$, these *inter*icosahedral modes form a distinct band above the continuous band. The secondary peak around 1100 cm^{-1} in the experimental spectra is ascribed to this, from which we can conclude that $\alpha_1>\alpha$ for amorphous boron. This supports the idea that the *inter*icosahedral bonding has largely covalent character, which is reasonable using the analogy with the crystal boron. The shape of the density of states at the low-frequency side also supports this. A relatively large noncentral force, which is a characteristic of the covalent bond, is assigned to the *inter*icosahedral bonds.

The highest secondary band exhibits both infrared and Raman activities. The symmetrical and antisymmetrical vibrations of these bonds, which have crucial significance in the crystal case, are averaged and hence the effects are less important on the vibrational responses in the amorphous spectra.

ACKNOWLEDGMENTS

We wish to acknowledge the support of Yamada Science Foundation, which made it possible for one of the authors (M.F.T.) to visit Japan.

*Also at Center for Fundamental Materials Research, Michigan State University.

[1] R. Zallen, *The Physics of Amorphous Solids* (Wiley, New York, 1983), Chap. 3.
[2] O. A. Golikova, Phys. Status Solidi A **51**, 11 (1979); C. C. Tsai, Phys. Rev. B **12**, 2041 (1979).
[3] A. A. Berezin, O. A. Golikova, M. M. Kazanin, T. Khomidov, D. N. Mirlin, A. V. Petrov, A. S. Umarov, and V. K. Zaitsev, J. Non-Cryst. Solids **16**, 237 (1974).
[4] N. Morita and A. Yamamoto, Jpn. J. Appl. Phys. **14**, 825 (1975).
[5] K. Shirai and S. Gonda, J. Phys. Chem. Solids **53**, 1081 (1992).
[6] A. R. Badzian, Mater. Res. Bull. **2**, 987 (1967).
[7] K. Katada, Jpn. J. Appl. Phys. **5**, 582 (1966); R. G. Delaplane, U. Dahlborg, B. Granéli, P. Fischer, and T. Lundström, J. Non-Cryst. Solids **104**, 249 (1988); M. Kobayashi, T. Oyama, H. Nishizawa, T. Ishii, and K. Takeuchi, J. Mater. Sci. Lett. **8**, 403 (1989).
[8] N. N. Greenwood, in *Comprehensive Inorganic Chemistry*, edited by J. C. Bailar, H. J. Emeléus, Sir R. Nyholm, and A. F. Trotman-Dickenson (Pergamon, Oxford, 1973), Chap. 11.
[9] M. Kobayashi, I. Higashi, and M. Takami, J. Solid State Chem. (to be published).
[10] K. Shirai, J. Solid State Chem. (to be published).
[11] H. Werheit, *Proceedings of the 9th International Conference on Boron, Borides and Related Compounds* (Universität Duisburg, Duisburg, 1987), pp. 142–151.
[12] U. Kuhlmann, H. Werheit, T. Lundström, and W. Robers, J. Phys. Chem. Solids **55**, 579 (1994).
[13] K. Shirai, S. Emura, S. Gonda, and Y. Kumashiro, J. Appl. Phys. **78**, 3392 (1995).
[14] P. A. Medwick, D. G. Cahill, A. K. Raychaudhuri, R. O. Pohl, F. Gomfp, N. Nücker, and T. Tanaka, in *Boron-Rich Solids*, edited by D. Emin *et al.*, AIP Conf. Proc. No. 231 (AIP, New York, 1991), pp. 363–370.
[15] M. F. Thorpe, in *Excitations in Disordered Systems*, edited by M. F. Thorpe (Plenum, New York, 1982), pp. 85–107.
[16] M. F. Thorpe, Phys. Rev. B **8**, 5352 (1973).
[17] M. F. Thorpe and F. L. Galeener, Phys. Rev. B **22**, 3078 (1980).
[18] R. B. Laughlin and J. D. Joannopoulos, Phys. Rev. B **16**, 2942 (1977).
[19] C. Domb, Adv. Phys. **9**, 149 (1960).
[20] K. Shirai, M. F. Thorpe, and S. Gonda, J. Non-Cryst. Solids **198-200**, 36 (1996).
[21] F. Yndurain, R. Barrio, R. J. Elliott, and M. F. Thorpe, Phys. Rev. B **28**, 3576 (1983); R. A. Barrio, G. G. Naumis, and C. Wang, J. Non-Cryst. Solids **182**, 22 (1995).
[22] R. J. Elliott, R. A. Barrio, and M. F. Thorpe, Kinam **4C**, 55 (1982).
[23] P. N. Keating, Phys. Rev. **145**, 637 (1966).
[24] A. A. Maradudin, in *Solid State Physics*, edited by F. Seitz and D. Turnbull (Academic, New York, 1966), Vol. 19, pp. 1–134.
[25] K. Shirai and S. Gonda, J. Phys. Chem. Solids **57**, 109 (1996).
[26] C. L. Beckel, M. Yousaf, M. Z. Fuka, S. Y. Raja, and N. Lu, Phys. Rev. B **44**, 2535 (1991).
[27] R. Zallen, Phys. Rev. **173**, 824 (1968).

[28] A. Alben, D. Weaire, J. E. Smith, and M. H. Brodsky, Phys. Rev. B **11**, 2271 (1975).
[29] K. Shirai (unpublished).
[30] K. Shirai, in *Transactions of the Materials Research Society of Japan*, edited by R. Yamamoto and H. Yamamoto (MRS-J, Kawasaki, 1996), pp. 478–481.
[31] A. A. Maradudin and E. Burstein, Phys. Rev. **164**, 1081 (1967).
[32] S. Go, H. Bilz, and M. Cardona, Phys. Rev. Lett. **34**, 580 (1975).
[33] U. Kuhlmann and H. Werheit, Phys. Status Solidi B **175**, 85 (1993); J. Alloys Comp. **205**, 87 (1994).